

Article

Atomistic origins of the limited phase stability of Cs-rich FACsPbI mixtures

Ariadni Boziki, Dominik J. Kubicki, Aditya Mishra, Simone Meloni,
Lyndon Emsley, Michael Grätzel, and Ursula Rothlisberger

Chem. Mater., **Just Accepted Manuscript** • DOI: 10.1021/acs.chemmater.0c00120 • Publication Date (Web): 21 Feb 2020

Downloaded from pubs.acs.org on February 22, 2020

Just Accepted

“Just Accepted” manuscripts have been peer-reviewed and accepted for publication. They are posted online prior to technical editing, formatting for publication and author proofing. The American Chemical Society provides “Just Accepted” as a service to the research community to expedite the dissemination of scientific material as soon as possible after acceptance. “Just Accepted” manuscripts appear in full in PDF format accompanied by an HTML abstract. “Just Accepted” manuscripts have been fully peer reviewed, but should not be considered the official version of record. They are citable by the Digital Object Identifier (DOI®). “Just Accepted” is an optional service offered to authors. Therefore, the “Just Accepted” Web site may not include all articles that will be published in the journal. After a manuscript is technically edited and formatted, it will be removed from the “Just Accepted” Web site and published as an ASAP article. Note that technical editing may introduce minor changes to the manuscript text and/or graphics which could affect content, and all legal disclaimers and ethical guidelines that apply to the journal pertain. ACS cannot be held responsible for errors or consequences arising from the use of information contained in these “Just Accepted” manuscripts.

Atomistic origins of the limited phase stability of Cs^+ -rich $\text{FA}_x\text{Cs}_{(1-x)}\text{PbI}_3$ mixtures

Ariadni Boziki,[†] Dominik J. Kubicki,^{‡,§} Aditya Mishra,[‡] Simone Meloni,^{†,||}
Lyndon Emsley,[‡] Michael Grätzel,[¶] and Ursula Rothlisberger^{*,†}

[†]*Laboratory of Computational Chemistry and Biochemistry, Institute of Chemical Sciences
and Engineering, École Polytechnique Fédérale de Lausanne, CH-1015 Lausanne,
Switzerland.*

[‡]*Laboratory of Magnetic Resonance, Institute of Chemical Sciences and Engineering, École
Polytechnique Fédérale de Lausanne, CH-1015 Lausanne, Switzerland.*

[¶]*Laboratory of Photonics and Interfaces, Institute of Chemical Sciences and Engineering,
École Polytechnique Fédérale de Lausanne, CH-1015 Lausanne, Switzerland.*

[§]*Current address: Cavendish Laboratory, JJ Thomson Avenue, Cambridge CB3 0HE,
United Kingdom.*

^{||}*Current address: Dipartimento di Scienze Chimiche e Farmaceutiche (DipSCF),
Università degli Studi di Ferrara - Unife, Via Luigi Borsari 46, I-44121, Ferrara, Italy.*

E-mail: ursula.roethlisberger@epfl.ch

Phone: +41 (0)21 693 03 21. Fax: +41 (0)21 693 03 20

Abstract

Mixed cation perovskites, $[\text{HC}(\text{NH}_2)_2]_x\text{Cs}_{(1-x)}\text{PbI}_3$, ($\text{FA}_x\text{Cs}_{(1-x)}\text{PbI}_3$) with $x = 0.8$ achieve high solar cell power conversion efficiencies (PCEs) while exhibiting long-term stability under ambient conditions. In this work, we perform density functional theory (DFT) calculations, first-principles molecular dynamics (MD) simulations, solid-state

nuclear magnetic resonance (NMR) and X-ray powder diffraction (XRD) measurements aimed at investigating the possible phase stability of Cs⁺-rich FA_xCs_(1-x)PbI₃, (0 ≤ x ≤ 0.5) mixed-cation materials as potential candidates for tandem solar cell applications. Estimations of the free energy of the mixtures with respect to the pure compounds together with calculations of the relative phase stability at 0 K and at finite temperature show that although the mixtures can form, the δ phase remains the thermodynamically most stable phase at room temperature. This is fully corroborated by solid-state NMR and XRD measurements and is in contrast to FA⁺-rich Cs/FA mixtures where small additions of Cs⁺ are sufficient to stabilize the perovskite phase at ambient conditions. The atomistic origin for this contrasting behavior arises from an energetic destabilization of the perovskite phase on the one hand caused by the incorporation of a large cation (FA⁺) into the relatively small host lattice of γ-CsPbI₃ and on the other hand is induced by the lower degree of distortion of the host lattice. These observations allow us to propose a new design principle for the preferential stabilization of the perovskite phase over the competing δ phase.

Introduction

Over the last years, organic-inorganic hybrid lead halide perovskites have attracted great attention due to their impressive photovoltaic performance.¹⁻⁷ However, the long-term stability of perovskite solar cells remains a major challenge in order to approach commercialization. Indeed, the most widely studied material of this type, CH₃NH₃PbI₃ (MAPbI₃) has a band gap of 1.5 eV,³ which is close to the single-junction optimum of 1.34 eV, based on Shockley's and Queisser's detailed balance considerations, with a theoretical efficiency limit of 33.16%.^{8,9} In fact MAPbI₃ cells fabricated by regulated nucleation and Ostwald recrystallization, reach an impressive PCE of 20.3%.¹⁰ Unfortunately, MAPbI₃ films decompose rapidly at 423 K due to the high volatility of MAI which is prone to be attacked by polar solvents, in particular water.⁷ In a similar vein, the perovskite phase of formamidinium lead triiodide HC(NH₂)₂PbI₃,

(FAPbI₃) has a band gap that different experimental measurements showed to lie within the range of 1.43-1.48 eV,^{7,11,12} even closer to the single-junction optimum, but the thermodynamically most stable phase at room temperature is the non-perovskite hexagonal δ -phase (yellow phase) and the transition to the perovskite phase only occurs at high temperatures ($T = 433$ K).¹³

Purely inorganic cesium lead trihalide perovskites could present an alternative since, for instance, CsPbBr₃ forms a perovskite structure at room temperature.¹⁴ However, CsPbBr₃ has a rather wide bandgap that different experimental measurements determined to be in the range of 2.25 - 2.36 eV.^{14,15} The perovskite phase of CsPbI₃, on the other hand has an experimental band gap of 1.73 eV,^{16,17} which is close to the optimum top cell band gap for tandem solar cells of 1.7 - 1.8 eV,¹⁸ which offers a promising way for increasing the efficiency with a minimal cost increase.¹⁹⁻²² Unfortunately, CsPbI₃ also crystallizes in a non-perovskite hexagonal, insulating phase, the yellow δ phase at room temperature.²³ While the δ phase of FAPbI₃ consists of face-sharing octahedra that are surrounded by the monovalent cations, the δ phase of CsPbI₃ consists of edge-sharing octahedra. CsPbI₃ undergoes a first order phase transition from the non-perovskite to a black perovskite phase only at 600 K.¹⁵

This black perovskite phase has been assumed to be cubic,¹⁵ however recently, Wang *et al.*²⁴ obtained β -CsPbI₃ films with an extended spectral response and enhanced stability. In addition, the synchrotron powder diffraction measurements of Stoumpos *et al.*²⁵ showed that on cooling down from temperatures above 633 K, the perovskite phase can be kinetically stable with the occurrence of tetragonal and orthorhombic structures at 533 K and 448 K, respectively. In addition, Lai *et al.*²⁶ also reported an orthorhombic perovskite phase for CsPbI₃ nanowires based on X-ray diffraction pattern measured at 300 K. Using X-ray diffraction and performing DFT calculations, Sutton *et al.*²⁷ demonstrated that at room temperature, an orthorhombic structure is the most stable among the black perovskite polymorphs of CsPbI₃, which however remains less stable than the yellow non-perovskite form. Table 1 summarizes the different CsPbI₃ and FAPbI₃ phases.

It has also been reported that CsPbI₃ can adopt a black phase at room temperature by adding HI during the preparation process without any noticeable change of the optical properties of the material.¹⁷ Despite this apparent success, the mechanism of stabilization of the black phase of CsPbI₃ by HI, remained unclear. It was only recently that Ke *et al.*²⁸ showed that the black phase does not correspond to pure CsPbI₃ but that a new compound, (CH₃)₂NH₂PbI₃ (DMAPbI₃) is formed, where dimethylammonium (DMA) is the HI catalyzed decomposition product of the acidic hydrolysis of the solvent dimethylformamide (DMF). In the same study, the stabilization of the black perovskite phase of CsPbI₃ through mixing with DMA was demonstrated. In particular, the mixed cation compound Cs_{0.7}DMA_{0.3}PbI₃ achieved a maximum PCE of 12.62% and has a band gap of around 1.7 eV.

Table 1: Different phases of CsPbI₃ and FAPbI₃^{23,27,29}

Crystal structure	Crystal system	Space group	Thermodynamic stability	Temperature range
δ -CsPbI ₃	orthorhombic	<i>Pnma</i>	stable	≤ 600 K
γ -CsPbI ₃	orthorhombic	<i>Pnam</i>	metastable	≤ 448 K
β -CsPbI ₃	tetragonal	<i>P4-<i>mbm</i></i>	metastable	448 K - 533 K
cubic-CsPbI ₃	cubic	<i>Pm-3<i>m</i></i>	stable	≥ 600 K
δ -FAPbI ₃	hexagonal	<i>P6₃mc</i>	stable	≤ 433 K
β -FAPbI ₃	trigonal	<i>P3</i>	metastable	≥ 150 K
α -FAPbI ₃	trigonal	<i>P3<i>m</i>1</i>	stable	≥ 433 K

Summarizing, although the most studied single-cation compounds possess band gaps either close to the optimum for single-junction or top cell in tandem solar cells, they are thermodynamically not stable in the perovskite phase over a sufficient temperature range. To overcome this problem, a design protocol has been introduced that mixes different monovalent cations and halides achieving an enhanced thermal and structural stability.³⁰⁻³²

Indeed, Pellet *et al.*³⁰ produced cells with an enhanced short-circuit current by using a mixture of FA⁺ and MA⁺ as monovalent cations. However, similar to MAPbI₃ films, the mixed compounds are also prone to decomposition at high temperatures. To circumvent problems related to thermal decomposition of MA⁺, cesium has attracted attention for use

1
2
3 in mixed organic-inorganic lead halide perovskites. Choi *et al.*³³ presented cesium-doped
4 MAPbI₃ cells, achieving an efficiency of 7.68% upon addition of 10% cesium. Moreover, Lee *et*
5 *al.*³⁴ presented mixtures of cesium and formamidinium with enhanced thermal and humidity
6 stability, achieving a power conversion efficiency of 16.5%. We have shown previously that
7 the addition of Cs⁺ into FAPbI₃ leads to a reduction of the phase transition temperature by
8 ~ 200 - 300 K, explaining why the perovskite phase becomes stable at room temperature for
9 Cs_xFA_(1-x)PbI₃ compounds.³⁵ Furthermore, Saliba *et al.* proposed a triple cation perovskite
10 compound, which consists of Cs⁺, FA⁺ and MA⁺, achieving a PCE of 18 %.³¹ Hence, it
11 appears that Cs⁺ is highly efficient in suppressing the black-to-yellow phase transition in
12 3D perovskites based on FA⁺ as the majority cation. Li *et al.*³⁶ suggested that tuning the
13 Goldschmidt tolerance factor^{37,38} and its extension to organic cations proposed by Kieslich *et*
14 *al.*,^{39,40} through solid-state alloying could be a way to stabilize the black perovskite structure.
15 Specifically, the authors report that by mixing FAPbI₃ with CsPbI₃, the effective tolerance
16 factor can be tuned and mixtures of low Cs⁺ concentration, which are stable in the perovskite
17 phase, can be formed.

18
19 In contrast to the FA⁺-rich case of FA/Cs mixtures, Cs⁺-rich compounds have been less
20 investigated so far although they might be promising candidates for tandem solar cells.¹⁹⁻²²
21 In this work, we set out to investigate the stability of Cs⁺-rich, FA_xCs_(1-x)PbI₃ mixtures, for
22 FA⁺ concentrations up to 50%, through a combination of DFT calculations, MD simulations
23 and experiments. The goal of our investigation is to examine if stable Cs⁺-rich mixtures
24 can be formed and if they lead to the desired stabilization of the perovskite phase. We
25 first evaluate the free energy for the mixtures with respect to the pure phases, in order to
26 establish if mixing is possible and if it leads to any preferential stabilization of the perovskite
27 phase with respect to the δ phase. In addition, the energy difference between the δ and the
28 perovskite phase at 0 K provides a first indication about the relative stability of the two
29 phases and MD simulations are used to gain information about the relative phase stability
30 at finite temperature. Taken the results of our studies together, we show that although stable
31
32

1
2
3 mixtures can be formed they do not lead to significant extensions of the stability range of
4 the perovskite phase. This is also corroborated by solid-state NMR and XRD measurements
5 which show the formation of stable mixed Cs/FA δ phases at room temperature. Evaluation
6 of the structural characteristics of the mixed compounds reveals possible reasons for this
7 contrasting behavior between FA⁺-rich versus Cs⁺-rich FA/Cs perovskites. Calculations of
8 the optical properties of the metastable Cs⁺-rich perovskite materials show that they would
9 be potential candidates for solar cells applications, motivating a search for alternative ways
10 of preparation.
11
12
13
14
15
16
17
18
19
20

21 Results and discussion

22 Properties of CsPbI₃

23
24
25 As mentioned above, it is now well-known that apart from the two thermodynamically
26 stable phases of CsPbI₃; a non-perovskite δ -phase from 0 up to 600 K and a cubic perovskite
27 phase above 600 K (Figure 1),¹⁵ two more kinetically stabilized black perovskite phases
28 with distorted octahedra have been observed. These phases are known as β and γ phases,
29 respectively, with the orthorhombic γ -CsPbI₃ (Figure 2) being the most stable one among the
30 perovskite polymorphs at room temperature, but still remaining less stable than the yellow
31 non-perovskite phase.^{25,27} For this reason, in our study we have taken the three phases, δ , γ
32 as well as the high temperature cubic phase into account.
33
34
35
36
37
38
39
40
41
42
43

44 The calculated single-particle Kohn-Sham band gap of the cubic perovskite phase within
45 the fully \mathbf{k} -point converged unit cell at 0 K, as predicted by calculations employing the PBE
46 functional,⁴¹ is 1.44 eV, in good agreement with other theoretical studies,^{42,43} but somewhat
47 in contrast to the experimentally measured band gap of 1.73 eV.^{16,17} To make a meaningful
48 comparison with the experimental data, which has been measured at finite temperature,
49 thermal effects should also be taken into account. The thermal effects can fully be taken
50 into account by performing first-principles MD simulations at finite temperature. For this
51
52
53
54
55
56
57
58
59
60

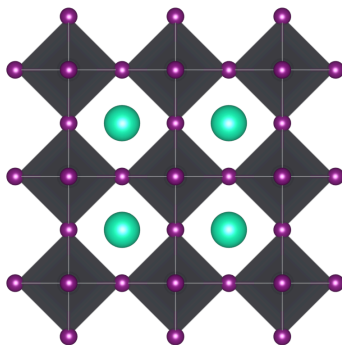


Figure 1: DFT optimized structure of cubic-CsPbI₃.

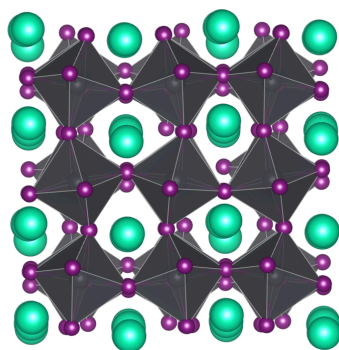


Figure 2: DFT optimized structure of the γ -CsPbI₃.

reason, we performed Car-Parrinello MD simulations of 5.4 ps in the NVT ensemble at a temperature of 300 K, for a cubic CsPbI₃ supercell of 320 atoms at the gamma point. The 0 K band gap of this real-space equivalent of the fully \mathbf{k} -point converged sample is 1.39 eV. Figure 3 shows the histogram of the band gaps for different finite temperature configurations, allowing to calculate the contribution of temperature effects on the 0 K band gap. We find that this contribution is as large as 0.49 eV. This is unusually large, since in previous studies, contributions of thermal effects to the band gap, for similar types of materials, are of the order of 0.15 eV.⁴⁴ However, it is worth mentioning that Wiktor *et al.*⁴² also estimated a 0.47 eV contribution of thermal effects to the 0 K gap of cubic CsPbI₃, employing the rVV10 functional.^{45,46} Summarizing, the calculated finite temperature band gap is 1.83 eV comparable with the experimental band gap.^{16,17}

Since the metastable γ -CsPbI₃ phase is the most stable among the different perovskite

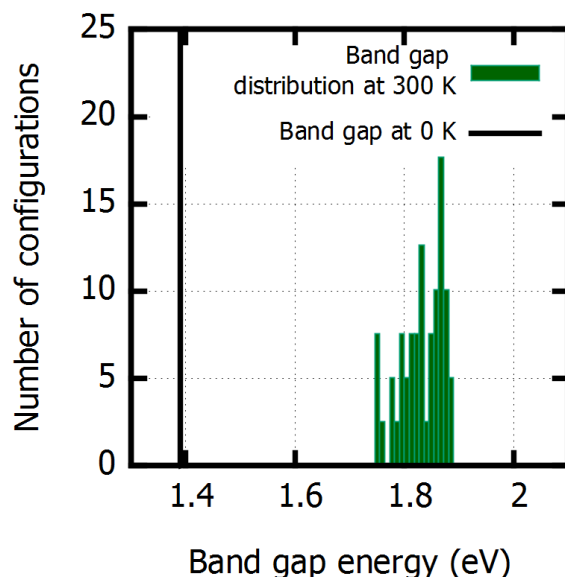


Figure 3: Histogram of the thermal distribution of the band gap compared to the value at 0 K for the cubic phase of CsPbI₃.

polymorphs at room temperature, we also examined the orthorhombic structure with a cell containing 240 atoms. The fully DFT optimized structure at 0 K has average Pb-I-Pb angles of 155° versus 154° of the experimental orthorhombic CsPbI₃.²⁷ The fully converged, \mathbf{k} -point sampled 0 K band gap is 1.77 eV. As shown in Figure S1 of Supporting Information, thermal effects at 300 K are much smaller than in the case of cubic-CsPbI₃ and amount to 0.1 eV only. The significant difference between the thermal effects of the cubic and the orthorhombic cell can be explained by considering the nature of the valence band maximum (VBM) which is formed by an antibonding combination of I p and Pb s orbitals.⁴³ In cubic-CsPbI₃, on the one hand, the distortions induced by the dynamic disorder of the lattice at finite temperature lead to a reduction of the antibonding overlap and in turn to an increase of the band gap. In γ -CsPbI₃, on the other hand, since the lattice is already orthorhombic the dynamic disorder at finite temperature induces only further distortions that lead to only a slight reduction of the antibonding overlap and a slight increase of the band gap, respectively. For completeness, we considered both the orthorhombic as well as the cubic phases in the subsequent investigation of the mixed-cation phases of FA_xCs_(1-x)PbI₃.

Mixed $\text{FA}_x\text{Cs}_{(1-x)}\text{PbI}_3$ compounds ($0 \leq x \leq 0.5$)

In order to study if mixed-cation compounds in the three phases δ , γ and cubic are stable and if any preferential phase stabilization takes place upon mixing, we performed structural relaxations (atomic positions and cell parameters) of the mixed $\text{FA}_x\text{Cs}_{(1-x)}\text{PbI}_3$ compounds at 0 K and computed the mixing internal energy and entropy. We remark that for computing the mixing internal energy of the perovskite phases we used β -FAPbI₃ as a reference.²³

$$\begin{aligned} \Delta E_{\text{phase}}(\text{FA}_x\text{Cs}_{(1-x)}\text{PbI}_3) &= E_{\text{phase}}(\text{FA}_x\text{Cs}_{(1-x)}\text{PbI}_3) \\ &- [xE_{\text{phase}}(\text{FAPbI}_3) \\ &+ (1-x)E_{\text{phase}}(\text{CsPbI}_3)] \end{aligned} \quad (1)$$

$$T\Delta S_{\text{phase}}(\text{FA}_x\text{Cs}_{(1-x)}\text{PbI}_3) = -k_B T [x \ln x + (1-x) \ln(1-x)] \quad (2)$$

Analysis of the energetic contribution to the mixing free energy, which is expressed by equation (1) shows that in the case of the δ phase, replacement of Cs^+ by FA^+ leads to destabilization (energy increase) with respect to the pure FA and/or CsPbI_3 δ phases (magenta line in Figure 4 upper panel). The mixing entropy contribution to the free energy expressed by equation (2) and calculated at room temperature, (298 K), only partially compensates this penalty. Similarly, in the γ phase, mixing induces almost no or slightly positive energetic contributions (Figure 4, bottom panel, magenta line) and the estimated free energy of mixing is close to zero (Figure 4, bottom panel, black line). Indeed, for both cases, δ and γ phases, (excluding only the δ - $\text{FA}_{0.33}\text{Cs}_{0.67}\text{PbI}_3$, where mixing leads to destabilization with respect to the pure phases) the estimated free energy of mixing is of the order of 0.006 eV per stoichiometric unit, which is smaller than the typical variations among different substitution patterns. Since these values lie within the intrinsic error of the calculations, we cannot conclude if mixing in orthorhombic γ and δ phases leads to marginally stable, or slightly unstable compounds with respect to the pure phases.

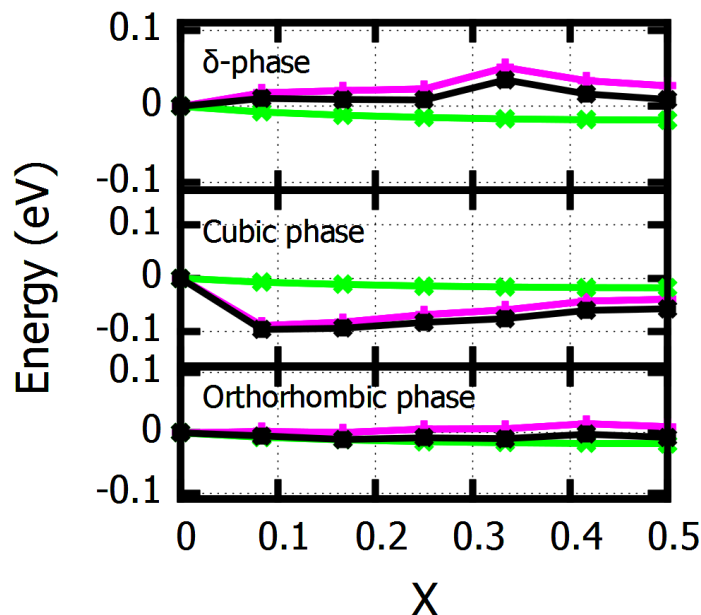


Figure 4: Variation of the free energy, of $\text{FA}_x\text{Cs}_{(1-x)}\text{PbI}_3$ expressed as $\Delta F = \Delta E - T\Delta S$ (black line), the internal energy, ΔE (magenta line), and the mixing entropy contribution, $-T\Delta S$ (with $T=298$ K, light-green line), as a function of FA^+ ratio. In the top graph the variations of free energy, enthalpy and mixing entropy contribution are estimated with respect to the pure δ phases. In the middle and bottom graphs each contribution to the free energy is estimated with respect to cubic- CsPbI_3 and γ - CsPbI_3 , respectively.

In contrast, cation mixing is already favored by the energetic contribution when cubic- CsPbI_3 is employed as reference, (Figure 4 central panel). As expected, the mixing entropy contribution further favors the stabilization of the perovskite phase, leading to a stability maximum around $\text{FA}_{0.08}\text{Cs}_{0.92}\text{PbI}_3$ with respect to the pure compounds. One should mention here that the calculation of any possible stabilization of the mixtures with respect to the cubic- CsPbI_3 does not imply that the mixtures adopt the cubic phase as well. In fact, cation mixing induces a sizable distortion on the cubic phase resulting in optimized structures of orthorhombic type for the mixtures, *i.e.* with all the three tilting angles different from zero.

An issue that demands further investigation is if the inclusion of zero point energy and vibrational entropy contributions influence the relative free energies. Calculations of the vibrational entropy term are not trivial in the case of perovskites. Indeed, both harmonic and quasi-harmonic phonon calculations lead to imaginary modes, which have no physical

1
2
3 meaning.⁴⁷ In our case, since we are considering relative stabilities within the same crystal-
4
5
6
7
8
9
10
11
12
13
14
15
16
17
18
19
20
21
22
23
24
25
26
27
28
29
30
31
32
33
34
35
36
37
38
39
40
41
42
43
44
45
46
47
48
49
50
51
52
53
54
55
56
57
58
59
60

meaning.⁴⁷ In our case, since we are considering relative stabilities within the same crystallographic phase, we consider these relative differences to a first approximation to be small but still able to influence the stability trend of the mixing free energy with respect to the pure phases.

We use the energy difference at 0 K as a first indicator of the relative stability of the perovskite and the δ phases. As shown in Table 2, δ -CsPbI₃ has a lower energy at 0 K, which is consistent with the experimental data that predict the δ phase to be the most stable low temperature phase.²³ However, when considering cation mixing in the cubic-CsPbI₃, FA⁺ substitution leads to a reduction of the energy difference by roughly half, independent of the FA⁺ doping level. On the contrary, FA⁺ mixing in γ -CsPbI₃ reduces the energy difference with the δ phase by only 14 - 21% up to 25% of FA⁺ and 21 - 36% for higher doping levels up to 50% FA⁺. As previously, the mixed-cation phases are orthorhombic rather than cubic as soon as the mixtures are generated, explaining why the energy differences with the δ phase for cubic and orthorhombic are the same at all FA⁺ contents. It is interesting to compare the effect of Cs⁺ mixing in FAPbI₃ with FA⁺ mixing in CsPbI₃. In the case of FAPbI₃, the most stable perovskite phase is the β one, which is more distorted with respect to the other known perovskite phase of FAPbI₃, the α phase. At variance with FA⁺ mixing into γ -CsPbI₃, Cs⁺ mixing in β -FAPbI₃ reduces the energy difference between the δ and the β FAPbI₃ phase at 0 K by only 8% for a doping level of 8% Cs⁺ and to 17% for doping levels up to 25% Cs⁺. For higher doping levels up to 50% Cs⁺, the energy difference is reduced by 33%. We also report the Goldschmidt tolerance factors of both the pure compounds and the mixtures (Table S1 of Supporting Information).

To shed more light on the finite temperature phase stability, we performed MD simulations at 300 K employing the *NVT* ensemble at the gamma point for δ and orthorhombic FA_{0.33}Cs_{0.67}PbI₃ compounds, using simulation cells of 176 atoms. From the average potential energy of an equilibrated trajectory of 2.2 ps, as shown in Figure 5, we conclude that the δ phase is still the more stable phase at room temperature. In addition, within the time scale of

Table 2: Relative energetic stability, expressed by $\Delta E_{a\delta} = E_a - E_\delta$ per stoichiometric unit of the cubic/orthorhombic perovskite phase with respect to the δ phase upon doping of CsPbI_3 with FA^+

Fraction of FA^+ doped into CsPbI_3 structure	Difference in energy (per stoichiometric unit) between perovskite and δ phases at 0 K (eV)	
	Reference structure cubic- CsPbI_3	Reference structure γ - CsPbI_3
0%	0.23	0.14
8%	0.12	0.12
17%	0.11	0.11
25%	0.12	0.12
33%	0.09	0.09
42%	0.11	0.11
50%	0.11	0.11

these simulations and taking into account that our systems are not containing any vacancies that could cause diffusion, no phase segregation towards the pure phases was observed. This behavior is expected, since as has been reported by previous studies the diffusion barriers for cations such as Cs^+ and FA^+ are very large and diffusion could only be observed on very long time scales.⁴⁸

We have verified the theoretical predictions by synthesizing $\text{FA}_{0.08}\text{Cs}_{0.92}\text{PbI}_3$ and $\text{FA}_{0.16}\text{Cs}_{0.84}\text{PbI}_3$ using solid-state mechano-synthesis⁴⁹⁻⁵¹ and characterizing them using solid-state magic angle spinning (MAS) NMR (Figure 6). Our group and others have previously shown that solid-state NMR,⁵²⁻⁶⁰ and in particular ^{133}Cs ,^{57,61-65} can be used to probe the atomic-level microstructure of halide perovskites. Cesium environments corresponding to Cs^+ incorporated into the 3D perovskite lattice of α - FAPbI_3 (Figure 6a, 13 ppm, FWHM (1169 ± 20) Hz), Cs^+ inside the black orthorhombic γ - CsPbI_3 3D perovskite (Figure 6b, 154 ppm, FWHM (440 ± 4) Hz) and yellow non-perovskite δ - CsPbI_3 , (Figure 6c, 242 ppm, FWHM (353 ± 4) Hz) are characterized by distinct and unambiguous shifts in ^{133}Cs MAS NMR spectra. The as-prepared powders of $\text{FA}_{0.08}\text{Cs}_{0.92}\text{PbI}_3$ and $\text{FA}_{0.16}\text{Cs}_{0.84}\text{PbI}_3$ are yellow and their color is not affected by annealing at 170 °C. Their spectra (Figure 6d, e) contain a peak which is identical to that of δ - CsPbI_3 , confirming the non-perovskite nature of these

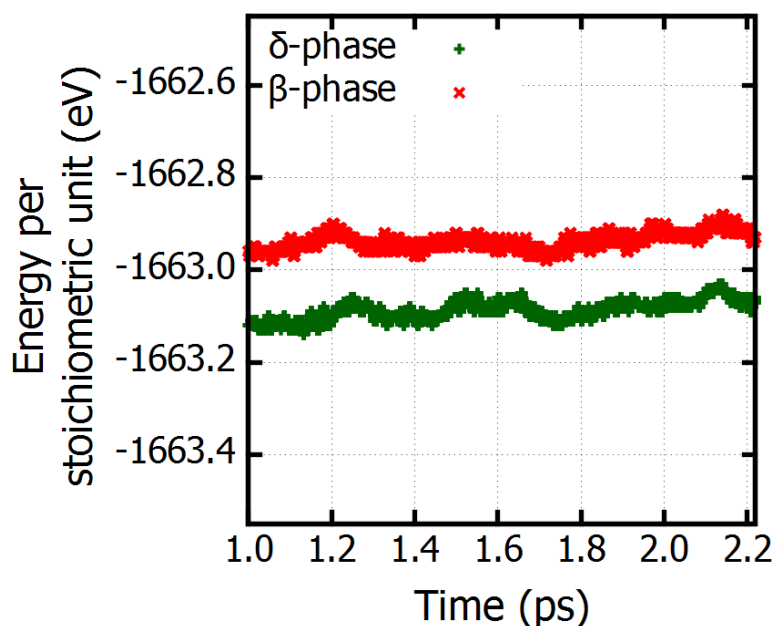


Figure 5: Potential energies per stoichiometric unit for each frame for the δ and the perovskite $\text{FA}_{0.33}\text{Cs}_{0.67}\text{PbI}_3$ mixtures across a 2.2 ps trajectory derived by MD simulations. The δ phase is always more stable than the perovskite one.

Cs^+ -rich $\text{FA}_x\text{Cs}_{(1-x)}\text{PbI}_3$ phases.

That said, in both spectra there is an overlapping broad component ($\text{FA}_{0.16}\text{Cs}_{0.84}\text{PbI}_3$: fitted shift of 236 ppm and FWHM (1885 ± 30) Hz) which corresponds to a distribution of structurally disordered cesium environments due to the incorporation of FA^+ into the non-perovskite δ - CsPbI_3 structure. We corroborate this hypothesis by measuring ^1H and ^{13}C CP MAS NMR spectra of the mixed-cation $\text{FA}_{0.16}\text{Cs}_{0.84}\text{PbI}_3$ material (Figure 6h, 6k) and comparing them to those of α - FAPbI_3 (Figure 6f, 6i) and δ - FAPbI_3 (Figure 6g, 6j). For both nuclei, the FA resonances of $\text{FA}_{0.16}\text{Cs}_{0.84}\text{PbI}_3$ are significantly shifted with respect to those of the reference phases, confirming that FA^+ is present in a new microscopically different chemical environment and that there is no phase segregation into pure α - FAPbI_3 or δ - FAPbI_3 , in contrast to previous experimental results, suggesting that for high Cs^+ concentrations, phase separation to the pure δ phases is observed.³⁶ We note that the ^1H peak at 11.3 ppm

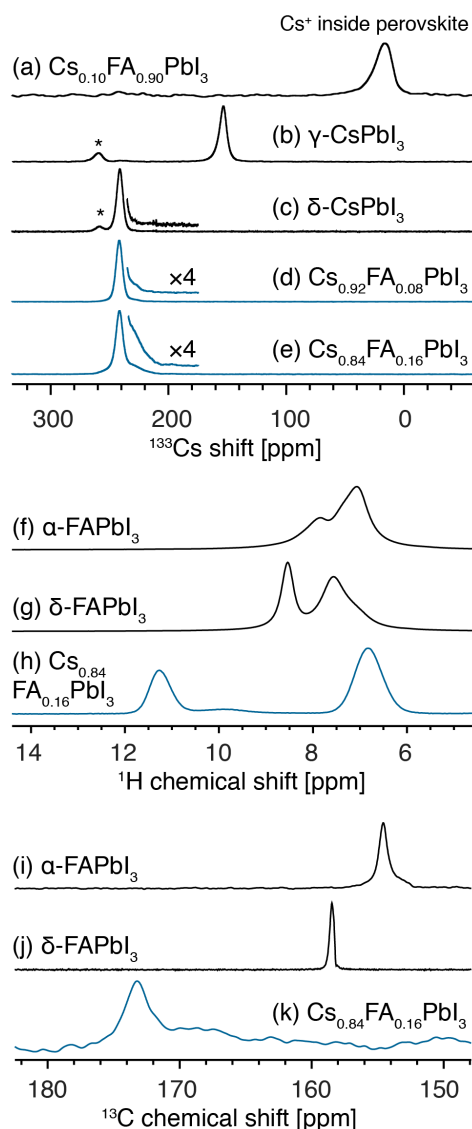


Figure 6: Solid-state MAS NMR characterization of the materials. ^{133}Cs spectra at 11.7 T, 298 K and 22 kHz MAS of (a) $\text{FA}_{0.9}\text{Cs}_{0.1}\text{PbI}_3$, (b) $\gamma\text{-CsPbI}_3$, (c) $\delta\text{-CsPbI}_3$, (d) $\text{FA}_{0.08}\text{Cs}_{0.92}\text{PbI}_3$, (e) $\text{FA}_{0.16}\text{Cs}_{0.84}\text{PbI}_3$. ^1H and ^{13}C spectra at 21.1 T, 100 K and 12 kHz MAS of (f, i) $\alpha\text{-FAPbI}_3$, (g, j) $\delta\text{-FAPbI}_3$, (h, k) $\text{FA}_{0.16}\text{Cs}_{0.84}\text{PbI}_3$. The asterisks (*) indicate an impurity phase (Cs_4PbI_6).⁶⁵

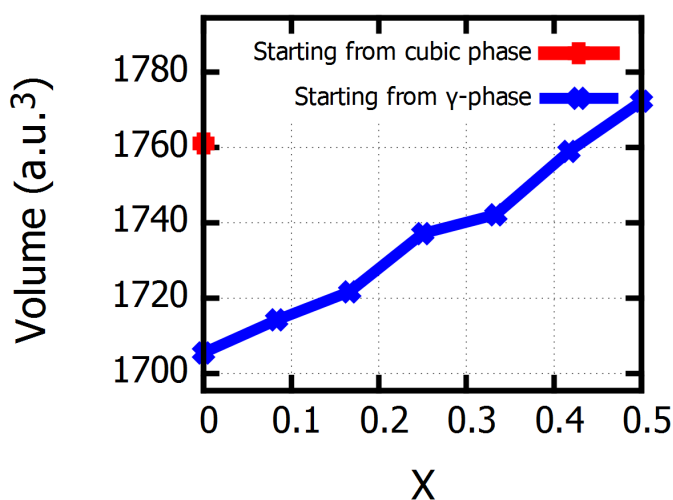
is likely a side product of the reaction when it is carried out at this stoichiometric ratio since it has a significantly different T_1 (23 s) than that of the FA peak (6.8 ppm, $T_1=14$ s). If the two peaks belonged to the same phase, ^1H - ^1H spin diffusion would act to equalize their relaxation times, which is not the case here. The solid-state NMR results are also consistent

1
2
3 with the XRD patterns of the materials (Figure S3, Figure S4 of Supporting Information),
4 whereby the mixed phases show reflections corresponding to δ -CsPbI₃ which are broadened
5 due to the presence of static chemical disorder. In addition, the longitudinal relaxation time,
6 T_1 , of FA in FA_{0.16}Cs_{0.84}PbI₃ is significantly longer (14 s) compared to that of α -FAPbI₃
7 (2.5 s) δ -FAPbI₃ (1 s). T_1 relaxation in protonated solids depends on the strength of the
8 ¹H-¹H dipolar interaction,⁶¹ and the spectral density at ¹H Larmor frequency. While the
9 dipolar interaction that drives relaxation is largely intramolecular and is not expected to
10 change between phases, differences in spectral density reflect the different extent of residual
11 motion present at 100 K. This allows us to further corroborate that the FA environments in
12 FA_{0.16}Cs_{0.84}PbI₃ are microscopically different than those of δ -FAPbI₃ and α -FAPbI₃.
13
14
15
16
17
18
19
20
21
22

23 Taken together, the theoretical analysis and the experimental results confirm that in
24 contrast to the FA⁺-rich case, Cs⁺-rich mixed perovskite phases are not thermodynamically
25 stable at room temperature. We therefore study the reasons why in contrast to the FA⁺-
26 rich case, mixing in the γ phase is enthalpically significantly disfavored. An analysis of the
27 structural characteristics of the mixed compounds allows us to rationalize the destabilization
28 of the Cs⁺-rich mixtures in the γ phase. The calculated volume per stoichiometric unit of
29 γ -CsPbI₃ (252.73 Å³) is 7.3 % smaller than that of α -FAPbI₃ (272.58 Å³). Upon FA⁺ doping
30 into the γ -CsPbI₃ lattice, the available volume for the monovalent cation is thus decreased.
31
32
33
34
35
36
37
38

39 In addition, following the evolution of the volume upon FA⁺ doping into CsPbI₃ (Figure
40 7), even in the case of cubic-CsPbI₃, we observe an abrupt decrease on going from the pure
41 compound to the lowest concentration (8 %), consistent with a transition from cubic to
42 orthorhombic phase, due to the lowering of symmetry and cubooctahedral distortion upon
43 cation substitution. This is also manifested in the average Pb-I-Pb angle distribution (Figure
44 8), which moves from an average of 180° (characteristic of the cubic phase) to 155° at low
45 FA⁺ doping ratios, indicating the adoption of an orthorhombic phase. This can again be
46 explained by the difference in ionic radii of Cs⁺ and FA⁺. In this case, the smaller Cs⁺ is
47 substituted by the larger FA⁺, imposing less distortions in the lattice. On increasing the
48
49
50
51
52
53
54
55
56
57
58
59
60

1
2
3 FA⁺ doping level, the volume of the cell is increasing proportionally, leading at 50 % of
4 doping to a volume which is larger than that of the initial cubic perovskite phase. The
5 inclusion of more FA⁺ alleviates the initial strain in the γ -CsPbI₃, which also explains the
6 gradual increase of the Pb-I-Pb angle distribution at high FA⁺ concentrations. Due to the
7 antibonding character of the VBM,⁴³ the reduction of the lattice distortion leads to an
8 increase of the overlap between the I p and Pb s orbitals (Figure 9), which in turn leads to
9 an energy increase (destabilization) of the mixed perovskite phases.
10
11
12
13
14
15
16
17



18
19
20
21
22
23
24
25
26
27
28
29
30
31
32
33
34
35 Figure 7: Volume evolution upon FA⁺ doping into CsPbI₃. Red and blue indicate results
36 obtained by starting from the pure cubic, respectively orthorhombic phase.
37
38

39
40 Having characterized the structural properties of the mixed-cation compounds, we now
41 turn to an analysis of their electronic properties. Several studies have shown that PBE-
42 GGA, without the inclusion of spin-orbit coupling effects (SOC) provides fortuitous good
43 predictions of the band gap of lead halide perovskites.^{66,67} Table 3 shows the evolution of
44 the calculated band gaps for the metastable perovskite phases, using this protocol. It is
45 obvious that upon mixing, the band gap remains remarkably unaffected, with values close
46 to the optimum for tandem solar cell applications. We observe that the highest band gap
47 values correspond to the most distorted orthorhombic structures, consistent with the well-
48 known electronic characteristics of the VBM of organic-inorganic lead halide perovskites, in
49
50
51
52
53
54
55
56
57
58
59
60

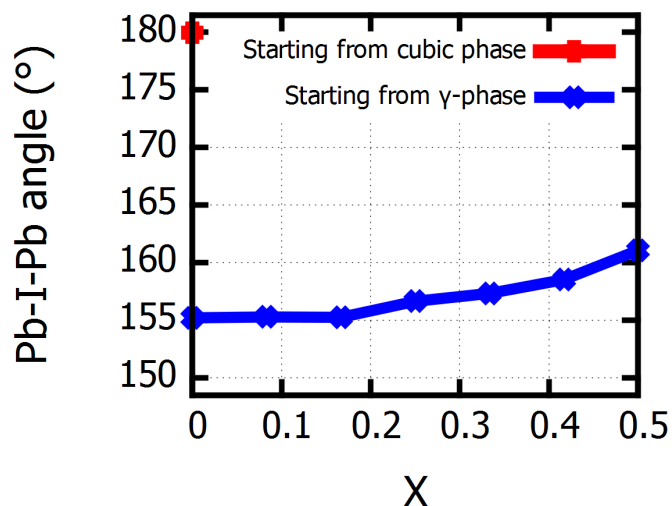


Figure 8: Average Pb-I-Pb angles evolution upon FA^+ doping into CsPbI_3 . Red and blue indicate results obtained by starting from the pure cubic, respectively orthorhombic phase.

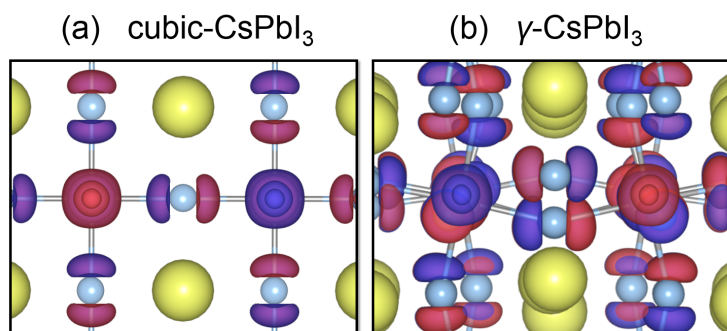


Figure 9: Antibonding overlap between the I p and Pb s orbitals of the VBM. Yellow, cyan and silver indicate Cs^+ , I^- and Pb^{2+} , respectively. The orbitals are represented with blue and red. Upon moving from the cubic structure (a) to the orthorhombic (b) the lattice distortion increases, leading to a reduction of the antibonding overlap.

which the overlap between I p and Pb s orbitals is reduced on going from the cubic to the orthorhombic phase.^{43,68}

Conclusions

The static DFT/PBE calculations, MD simulations, solid-state NMR and XRD measurements show that in contrast to the FA^+ -rich case, the perovskite phase of Cs^+ -rich $\text{FA}_x\text{Cs}_{(1-x)}\text{PbI}_3$ mixtures ($0 \leq x \leq 0.5$) is thermodynamically unstable at room temperature.

Table 3: Average DFT/PBE 0 K band gaps of cubic/orthorhombic CsPbI₃ and of Cs⁺-rich FA_xCs_(1-x)PbI₃ mixtures as a function of different FA⁺ concentrations. The standard deviation indicates variations due to different substitution patterns.

Fraction of FA ⁺ into CsPbI ₃	Band gap (eV)
0%	1.44 (cubic-CsPbI ₃)
0%	1.77 (γ -CsPbI ₃)
8%	1.81
17%	1.81 \pm 0.03
25%	1.80 \pm 0.02
33%	1.79 \pm 0.02
42%	1.79 \pm 0.01
50%	1.74 \pm 0.03

The energy difference between the δ and γ phases at 0 K, shows that the δ phase is more stable for both the pure and the mixed compounds. Furthermore, MD simulations at room temperature predict that the mixtures are stable at least within the time scale of the simulations and that the δ phase is preferred. This observation is also supported by solid-state NMR and XRD measurements suggesting that stable mixed-cation phases are formed and adopt the δ phase.

The contrasting behavior between FA⁺-rich and Cs⁺-rich FA_xCs_(1-x)PbI₃ mixtures can be explained in terms of the enthalpic penalty caused through the incorporation of the relatively large FA⁺ cation into the limited available space of the γ -CsPbI₃ orthorhombic lattice that enforces a structural transition towards a more cubic-like lattice where the space for the monovalent cation is larger. This structural change increases the antibonding overlap of the I p-orbitals with the s-orbitals of Pb of the VBM leading to a less stable structure. This behavior is contrary to the FA⁺-rich case, where the incorporation of Cs⁺ into α -FAPbI₃ leads to a distortion of the cubic host lattice towards a more orthorhombic structure, in which the antibonding overlap of the I p-orbitals with the s-orbitals of Pb of the VBM is lowered, leading to a more stable structure with larger band gap. These observations suggest a new design principle for the maximization of the preferential stabilization of the perovskite

1
2
3 phase over the competing δ phases. According to which, there is a higher chance to favor
4 the stabilization of the perovskite phase over the δ phase by using cubic-like phases as the
5 host lattice. On the contrary, the incorporation of a large cation into a relatively small and
6 already distorted 3D perovskite lattice reduces the stabilization of the perovskite phase over
7 the δ phase. Finally, the calculation of the band gaps of the mixed compounds indicates
8 that if the perovskite phase can be kinetically trapped, it would be a potential candidate for
9 tandem solar cell applications.
10
11
12
13
14
15
16
17
18

19 Computational details

20
21
22 DFT^{69,70} calculations have been performed using the Quantum Espresso suites of codes.^{71,72}
23 The Generalized Gradient Approximation (GGA) to DFT in the Perdew-Burke-Ernzerhof
24 (PBE) formulation has been used.⁴¹ The interactions between valence electrons and core
25 electrons and nuclei are described by ultrasoft pseudopotentials.⁷³ The Kohn-Sham orbitals
26 are expanded in a plane wave basis set with a kinetic energy cutoff of 40 Ry and a density
27 cutoff of 240 Ry. The Brillouin zone is sampled with a 4x4x4 Monkhorst-Pack k-points shifted
28 grid.⁷⁴ These values have been chosen after having performed convergence tests for the total
29 energy, the band gap, the pressure, the stresses and the atomic forces. SOC effects are not
30 explicitly included in the calculations due to the well-known fortuitous error cancellation of
31 SOC and many-body effects in the case of lead halide perovskites.⁶⁶
32
33
34
35
36
37
38
39
40
41

42 Comparing the absolute energy of Kohn-Sham orbitals in solid state systems is not trivial
43 since for an infinitely periodic system there is no reference value for the energy origin. A
44 technique to cope with this problem is to use localized deep impurity states or states that
45 are expected to be unaffected by the chemical and structural nature of the system such as
46 semicore or core states. As a reference, an approach analogous to the one used by Alkauskas
47 *et al.*⁷⁵ for band alignment in solids has been employed here, where the energy of the Pb_{5d}
48 semicore state is used as reference.⁴³ This is the only band which is rigidly shifted, something
49
50
51
52
53
54
55
56
57
58
59
60

1
2
3 that supports the idea that the vacuum level of these atomic orbitals is independent of the
4 system.⁴³
5
6

7 For the mixed compounds, the structures have been prepared starting from the experi-
8 mental cubic phase of CsPbI₃, replacing Cs⁺ by FA⁺ in different ratios. All the structures
9 consist of superlattices that contain 12 stoichiometric units. For each stoichiometry, when
10 allowed, we considered 10 different possible replacements, starting from the energetically low-
11 est configuration at the next lower FA⁺ content. The structures were fully relaxed (atomic
12 positions and cell parameters). The maximum standard deviation of the difference in energy
13 per stoichiometric unit among the different configurations is of the order of 0.006 eV.
14
15
16
17
18
19
20

21 Car-Parrinello MD simulations in the *NVT* ensemble were performed using the CPMD
22 code.⁷⁶ The wavefunction cutoff was set to 90 Ry and Goedecker normconserving pseudopo-
23 tentials were used.⁷⁷⁻⁷⁹ A time step of 5 a.u. was used with a fictitious mass parameter of
24 800 a.u.. The temperature in the simulations was set to 300 K and was controlled by a
25 Nosé-Hoover thermostat with a coupling frequency of 1000 cm⁻¹.⁸⁰⁻⁸²
26
27
28
29
30
31
32

33 Experimental details

34
35
36 **Perovskite mechanosynthesis:** Starting materials were stored inside a glove box under
37 argon. Perovskite powders were synthesized by grinding the reactants in an electric ball mill
38 (Retsch Ball Mill MM-200) using a grinding jar (10 ml) and a ball (ø10 mm) for 30 min at
39 25 Hz. The resulting powders were annealed for 5 minutes at temperatures specified below.
40
41
42
43
44 The amounts of reagents taken into the synthesis were as follows:
45
46

- 47 • δ -FAPbI₃: 0.172 g formamidinium hydroiodide (1.00 mmol) and 0.461 g PbI₂ (1.00
48 mmol). No annealing.
49
- 50 • α -FAPbI₃: δ -FAPbI₃ was annealed at 170 °C to induce the phase transition
51
- 52 • δ -CsPbI₃: 0.260 g CsI (1.00 mmol) and 0.461 g PbI₂ (1.00 mmol). No annealing
53
54
55
56
57

- γ -CsPbI₃: δ -CsPbI₃ was annealed at 350 °C to induce the phase transition to the α phase. After cooling to room temperature the black γ phase is obtained and the material transforms back to the δ phase with a half-life of about 1 hour.
- FA_{0.9}Cs_{0.1}PbI₃: 0.154 g of FAI (0.90 mmol), 0.026 g of CsI (0.10 mmol) and 0.461 g of PbI₂ (1.00 mmol). The material was annealed at 120 °C.
- FA_{0.08}Cs_{0.92}PbI₃: 0.014 g of FAI (0.08 mmol), 0.234 g of CsI (0.90 mmol) and 0.461 g of PbI₂ (1.00 mmol). The material was annealed at 170 °C.
- FA_{0.16}Cs_{0.84}PbI₃: 0.028 g of FAI (0.16 mmol), 0.218 g of CsI (0.84 mmol) and 0.461 g of PbI₂ (1.00 mmol). The material was annealed at 170 °C.

Solid-state NMR measurements: Room temperature ¹³³Cs (65.6 MHz) NMR spectra were recorded on a Bruker Avance III 11.7 T spectrometer equipped with a 3.2 mm CPMAS probe. Low-temperature ¹H (900 MHz) and ¹³C (225 MHz) NMR spectra were recorded on a Bruker Avance Neo 21.1 T spectrometer equipped with a 3.2 mm low-temperature CPMAS probe. ¹³³Cs shifts were referenced to 1 M aqueous solution of CsCl, using solid CsI (δ =271.05 ppm) as a secondary reference. ¹H and ¹³C chemical shifts were referenced to solid adamantane (δ_H =1.91 ppm and δ_C =29.45 (CH) and 38.48 (CH₂) ppm). Low-temperature ¹H-³¹P cross-polarization (CP) experiments used 1 ms optimized contact pulses, 63 kHz SPINAL-64 ¹H decoupling and the following recycle delays: 1.7 s (δ -FAPbI₃), 3 s (α -FAPbI₃), 22 s (FA_{0.16}Cs_{0.84}PbI₃). Quantitative echo-detected ¹³³Cs spectra used a recycle delay of 400 s. ¹H spectra were acquired with recycle delays between 2 and 20 s. Peak widths were fitted in Topspin 3.2 and the uncertainties are given at one standard deviation.

Conflicts of interest

”There are no conflicts to declare”.

Acknowledgement

U.R. gratefully acknowledges funding from the Swiss National Science Foundation via individual grant No. 200020-185092, the NCCR MUST and the Sinergia grant EPISODE. D.J.K, A.M. and L.E. are grateful for financial support from Swiss National Science Foundation Grant No. 200020_178860. The authors thank the Swiss National Supercomputing Centre (CSCS) for the computer time.

Supporting Information Available

Additional data from the MD simulations of γ -CsPbI₃, perovskite and δ FA_{0.33}Cs_{0.67}PbI₃. Goldschmidt tolerance factors for both the pure compounds and the mixtures. Powder XRD characterization of the pure compounds and the mixtures. Simulated powder XRD patterns.

References

- (1) Kojima, A.; Teshima, K.; Shirai, Y.; Miyasaka, T. Organometal Halide Perovskites as Visible-Light Sensitizers for Photovoltaic Cells. *J. Am. Chem. Soc.* **2009**, *131*, 6050–6051.
- (2) Im, J.-H.; Lee, C.-R.; Lee, J.-W.; Park, S.-W.; Park, N.-G. 6.5% Efficient Perovskite Quantum-Dot-Sensitized Solar Cell. *Nanoscale* **2011**, *3*, 4088–4093.
- (3) Kim, H.-S.; Lee, C.-R.; Im, J.-H.; Lee, K.-B.; Moehl, T.; Marchioro, A.; Moon, S.-J.; Humphry-Baker, R.; Yum, J.-H.; Moser, J. E.; Grätzel, M.; Park, N.-G. Lead Iodide Perovskite Sensitized All-Solid-State Submicron Thin Film Mesoscopic Solar Cell with Efficiency Exceeding 9%. *Sci. Rep.* **2012**, *2*, 591.
- (4) Lee, M. M.; Teuscher, J.; Miyasaka, T.; Murakami, T. N.; Snaith, H. J. Efficient Hybrid

- 1
2
3 Solar Cells Based on Meso-Superstructured Organometal Halide Perovskites. *Science*
4 **2012**, *338*, 643–647.
5
6
7
- 8 (5) Etgar, L.; Gao, P.; Xue, Z.; Peng, Q.; Chandiran, A. K.; Liu, B.; Nazeeruddin, M. K.;
9 Grätzel, M. Mesoscopic CH₃NH₃PbI₃/TiO₂ Heterojunction Solar Cells. *J. Am. Chem.*
10 *Soc.* **2012**, *134*, 17396–17399.
11
12
13
- 14 (6) Mei, A.; Li, X.; Liu, L.; Ku, Z.; Liu, T.; Rong, Y.; Xu, M.; Hu, M.; Chen, J.; Yang, Y.;
15 Grätzel, M.; Han, H. A Hole-Conductor-Free, Fully Printable Mesoscopic Perovskite
16 Solar Cell with High Stability. *Science* **2014**, *345*, 295–298.
17
18
19
- 20 (7) Eperon, G. E.; Stranks, S. D.; Menelaou, C.; Johnston, M. B.; Herz, L. M.; Snaith, H. J.
21 Formamidinium Lead Trihalide: a Broadly Tunable Perovskite for Efficient Planar
22 Heterojunction Solar Cells. *Energy Environ. Sci.* **2014**, *7*, 982–988.
23
24
25
- 26 (8) Shockley, W.; Queisser, H. J. Detailed Balance Limit of Efficiency of p-n Junction Solar
27 Cells. *J. Appl. Phys.* **1961**, *32*, 510–519.
28
29
30
- 31 (9) Rühle, S. Tabulated Values of the Shockley–Queisser Limit for Single Junction Solar
32 Cells. *Sol. Energy* **2016**, *130*, 139–147.
33
34
35
- 36 (10) Huang, Z.; Wang, D.; Wang, S.; Zhang, T. Highly Efficient and Stable MAPbI₃ Per-
37 ovskite Solar Cell Induced by Regulated Nucleation and Ostwald Recrystallization.
38 *Materials* **2018**, *11*, 778.
39
40
41
- 42 (11) Pang, S.; Hu, H.; Zhang, J.; Lv, S.; Yu, Y.; Wei, F.; Qin, T.; Xu, H.; Liu, Z.; Cui, G.
43 NH₂CH=NH₂PbI₃: An Alternative Organolead Iodide Perovskite Sensitizer for Meso-
44 scopic Solar Cells. *Chem. Mater.* **2014**, *26*, 1485–1491.
45
46
47
- 48 (12) Koh, T. M.; Fu, K.; Fang, Y.; Chen, S.; Sum, T. C.; Mathews, N.; Mhaisalkar, S. G.;
49 Boix, P. P.; Baikie, T. Formamidinium-Containing Metal-Halide: An Alternative Ma-
50
51
52
53
54
55
56
57
58
59
60

- 1
2
3 terial for Near-IR Absorption Perovskite Solar Cells. *J. Phys. Chem. C* **2014**, *118*,
4 16458–16462.
5
6
7
- 8 (13) Jeon, N. J.; Noh, J. H.; Yang, W. S.; Kim, Y. C.; Ryu, S.; Seo, J.; Seok, S. I. Composi-
9 tional Engineering of Perovskite Materials for High-Performance Solar Cells. *Nature*
10 **2015**, *517*, 476.
11
12
13
- 14 (14) Stoumpos, C. C.; Malliakas, C. D.; Peters, J. A.; Liu, Z.; Sebastian, M.; Im, J.;
15 Chasapis, T. C.; Wibowo, A. C.; Chung, D. Y.; Freeman, A. J.; Wessels, B. W.;
16 Kanatidis, M. G. Crystal Growth of the Perovskite Semiconductor CsPbBr₃: A New
17 Material for High-Energy Radiation Detection. *Cryst. Growth Des.* **2013**, *13*, 2722–
18 2727.
19
20
21
22
23
- 24 (15) Trots, D. M.; Myagkota, S. V. High-Temperature Structural Evolution of Caesium and
25 Rubidium Triiodoplumbates. *J. Phys. Chem. Solids* **2008**, *69*, 2520–2526.
26
27
28
29
- 30 (16) Møller, C. K. Crystal Structure and Photoconductivity of Caesium Plumbohalides.
31 *Nature* **1958**, *182*, 1436–1436.
32
33
34
- 35 (17) Eperon, G. E.; Paternò, G. M.; Sutton, R. J.; Zampetti, A.; Haghighirad, A. A.; Ca-
36 cialli, F.; Snaith, H. J. Inorganic Caesium Lead Iodide Perovskite Solar Cells. *J. Mater.*
37 *Chem. A* **2015**, *3*, 19688–19695.
38
39
40
41
- 42 (18) Coutts, T. J.; Emery, K. A.; Scott Ward, J. Modeled Performance of Polycrystalline
43 Thin-Film Tandem Solar Cells. *Prog Photovolt* **2002**, *10*, 195–203.
44
45
46
- 47 (19) Bailie, C. D.; Christoforo, M. G.; Mailoa, J. P.; Bowring, A. R.; Unger, E. L.;
48 Nguyen, W. H.; Burschka, J.; Pellet, N.; Lee, J. Z.; Grätzel, M.; Noufi, R.; Buonas-
49 sisi, T.; Salleo, A.; McGehee, M. D. Semi-Transparent Perovskite Solar Cells for
50 Tandems with Silicon and CIGS. *Energy Environ. Sci.* **2015**, *8*, 956–963.
51
52
53
54
55
56
57
58
59
60

- 1
2
3 (20) Todorov, T.; Gershon, T.; Gunawan, O.; Sturdevant, C.; Guha, S. Perovskite-Kesterite
4 Monolithic Tandem Solar Cells with High Open-Circuit Voltage. *Appl. Phys. Lett.* **2014**,
5 *105*, 173902.
6
7
8
9
10 (21) Bailie, C. D.; McGehee, M. D. High-Efficiency Tandem Perovskite Solar Cells. *MRS*
11 *Bull.* **2015**, *40*, 681–686.
12
13
14 (22) Leijtens, T.; Bush, K. A.; Prasanna, R.; McGehee, M. D. Opportunities and Challenges
15 for Tandem Solar Cells using Metal Halide Perovskite Semiconductors. *Nat. Energy*
16 **2018**, 2058–7546.
17
18
19
20
21 (23) Stoumpos, C. C.; Malliakas, C. D.; Kanatzidis, M. G. Semiconducting Tin and Lead
22 Iodide Perovskites with Organic Cations: Phase Transitions, High Mobilities, and Near-
23 Infrared Photoluminescent Properties. *Inorg. Chem.* **2013**, *52*, 9019–9038.
24
25
26
27 (24) Wang, Y.; Dar, M. I.; Ono, L. K.; Zhang, T.; Kan, M.; Li, Y.; Zhang, L.; Wang, X.;
28 Yang, Y.; Gao, X., et al. Thermodynamically Stabilized β -CsPbI₃-Based Perovskite
29 Solar Cells with Efficiencies >18%. *Science* **2019**, *365*, 591–595.
30
31
32
33 (25) Stoumpos, C. C.; Kanatzidis, M. G. The Renaissance of Halide Perovskites and Their
34 Evolution as Emerging Semiconductors. *Acc. Chem. Res.* **2015**, *48*, 2791–2802.
35
36
37 (26) Lai, M.; Kong, Q.; Bischak, C. G.; Yu, Y.; Dou, L.; Eaton, S. W.; Ginsberg, N. S.;
38 Yang, P. Structural, Optical, and Electrical Properties of Phase-Controlled Cesium
39 Lead Iodide Nanowires. *Nano Res.* **2017**, *10*, 1107–1114.
40
41
42
43 (27) Sutton, R. J.; Filip, M. R.; Haghighirad, A. A.; Sakai, N.; Wenger, B.; Giustino, F.;
44 Snaith, H. J. Cubic or Orthorhombic? Revealing the Crystal Structure of Metastable
45 Black-Phase CsPbI₃ by Theory and Experiment. *ACS Energy Letters* **2018**, *3*, 1787–
46 1794.
47
48
49
50
51
52
53
54
55
56
57
58
59
60

- 1
2
3 (28) Ke, W.; Spanopoulos, I.; Stoumpos, C. C.; Kanatzidis, M. G. Myths and Reality of
4 HPbI₃ in Halide Perovskite Solar Cells. *Nat. Commun.* **2018**, *9*, 4785.
5
6
7
8 (29) Wang, Y.; Dar, M. I.; Ono, L. K.; Zhang, T.; Kan, M.; Li, Y.; Zhang, L.; Wang, X.;
9 Yang, Y.; Gao, X.; Qi, Y.; Grätzel, M.; Zhao, Y. Thermodynamically Stabilized β -
10 CsPbI₃-Based Perovskite Solar Cells with Efficiencies >18%. *Science* **2019**, *365*, 591–
11 595.
12
13
14
15
16 (30) Pellet, N.; Gao, P.; Gregori, G.; Yang, T.-Y.; Nazeeruddin, M. K.; Maier, J.; Grätzel, M.
17 Mixed-Organic-Cation Perovskite Photovoltaics for Enhanced Solar-Light Harvesting.
18 *Angew. Chem.* **2014**, *53*, 3151–3157.
19
20
21
22
23 (31) Saliba, M.; Matsui, T.; Seo, J.-Y.; Domanski, K.; Correa-Baena, J.-P.; Nazeerud-
24 din, M. K.; Zakeeruddin, S. M.; Tress, W.; Abate, A.; Hagfeldt, A.; Grätzel, M. Cesium-
25 Containing Triple Cation Perovskite Solar Cells: Improved Stability, Reproducibility
26 and High Efficiency. *Energy Environ. Sci.* **2016**, *9*, 1989–1997.
27
28
29
30
31
32 (32) Saliba, M.; Matsui, T.; Domanski, K.; Seo, J.-Y.; Ummadisingu, A.; Zakeeruddin, S. M.;
33 Correa-Baena, J.-P.; Tress, W. R.; Abate, A.; Hagfeldt, A.; Grätzel, M. Incorporation
34 of Rubidium Cations into Perovskite Solar Cells Improves Photovoltaic Performance.
35 *Science* **2016**, *354*, 206–209.
36
37
38
39
40
41 (33) Choi, H.; Jeong, J.; Kim, H.-B.; Kim, S.; Walker, B.; Kim, G.-H.; Kim, J. Y. Cesium-
42 Doped Methylammonium Lead Iodide Perovskite Light Absorber for Hybrid Solar Cells.
43 *Nano Energy* **2014**, *7*, 80–85.
44
45
46
47 (34) Lee, J.-W.; Kim, D.-H.; Kim, H.-S.; Seo, S.-W.; Cho, S. M.; Park, N.-G. Formamidinium
48 and Cesium Hybridization for Photo- and Moisture-Stable Perovskite Solar Cell. *Adv.*
49 *Energy Mater.* **2015**, *5*, 1501310.
50
51
52
53
54 (35) Yi, C.; Luo, J.; Meloni, S.; Boziki, A.; Ashari-Astani, N.; Grätzel, C.; Zakeerud-
55 din, S. M.; Röthlisberger, U.; Grätzel, M. Entropic Stabilization of Mixed A-Cation
56
57
58
59
60

- 1
2
3 ABX₃ Metal Halide Perovskites for High Performance Perovskite Solar Cells. *Energy*
4 *Environ. Sci.* **2016**, *9*, 656–662.
5
6
7
8 (36) Li, Z.; Yang, M.; Park, J.-S.; Wei, S.-H.; Berry, J. J.; Zhu, K. Stabilizing Perovskite
9 Structures by Tuning Tolerance Factor: Formation of Formamidinium and Cesium Lead
10 Iodide Solid-State Alloys. *Chem. Mater.* **2016**, *28*, 284–292.
11
12
13
14 (37) Goldschmidt, V. M. Die Gesetze der Krystallochemie. *Naturwissenschaften* **1926**, *14*,
15 477–485.
16
17
18
19 (38) Mitzi, D. B. Templating and Structural Engineering in Organic–Inorganic Perovskites.
20 *J. Chem. Soc., Dalton Trans.* **2001**, 1–12.
21
22
23
24 (39) Kieslich, G.; Sun, S.; Cheetham, A. K. Solid-State Principles Applied to Or-
25 ganic–Inorganic Perovskites: New Tricks for an Old Dog. *Chem. Sci.* **2014**, *5*, 4712–
26 4715.
27
28
29
30
31 (40) Kieslich, G.; Sun, S.; Cheetham, A. K. An Extended Tolerance Factor Approach for
32 Organic-Inorganic Perovskites. *Chem. Sci.* **2015**, *6*, 3430–3433.
33
34
35
36 (41) Perdew, J. P.; Burke, K.; Wang, Y. Generalized Gradient Approximation for the
37 Exchange-Correlation Hole of a Many-Electron System. *Phys. Rev. B* **1996**, *54*, 16533–
38 16539.
39
40
41
42 (42) Wiktor, J.; Rothlisberger, U.; Pasquarello, A. Predictive Determination of Band Gaps
43 of Inorganic Halide Perovskites. *J. Phys. Chem. Lett.* **2017**, *8*, 5507–5512.
44
45
46
47 (43) Meloni, S.; Palermo, G.; Ashari-Astani, N.; Grätzel, M.; Rothlisberger, U. Valence and
48 Conduction Band Tuning in Halide Perovskites for Solar Cell Applications. *J. Mater.*
49 *Chem. A* **2016**, *4*, 15997–16002.
50
51
52
53
54
55
56
57
58
59
60

- 1
2
3
4 (44) Dar, M. I.; Jacopin, G.; Meloni, S.; Mattoni, A.; Arora, N.; Boziki, A.; Zakeeruddin, S. M.; Rothlisberger, U.; Grätzel, M. Origin of Unusual Bandgap Shift and Dual
5
6 Emission in Organic-Inorganic Lead Halide Perovskites. *Sci. Adv.* **2016**, *2*, e1601156.
7
8
9
10 (45) Vydrov, O. A.; Van Voorhis, T. Nonlocal Van der Waals Density Functional: The
11
12 simpler the Better. *J. Chem. Phys.* **2010**, *133*, 244103.
13
14 (46) Sabatini, R.; Gorni, T.; de Gironcoli, S. Nonlocal Van der Waals Density Functional
15
16 Made Simple and Efficient. *Phys. Rev. B* **2013**, *87*, 041108.
17
18
19 (47) Brivio, F.; Frost, J. M.; Skelton, J. M.; Jackson, A. J.; Weber, O. J.; Weller, M. T.;
20
21 Goñi, A. R.; Leguy, A. M. A.; Barnes, P. R. F.; Walsh, A. Lattice Dynamics and Vibra-
22
23 tional Spectra of the Orthorhombic, Tetragonal, and Cubic Phases of Methylammonium
24
25 Lead Iodide. *Phys. Rev. B* **2015**, *92*, 144308.
26
27
28 (48) Meloni, S.; Moehl, T.; Tress, W.; Frankevičius, M.; Saliba, M.; Lee, Y. H.; Gao, P.;
29
30 Nazeeruddin, M. K.; Zakeeruddin, S. M.; Rothlisberger, U., et al. Ionic Polarization-
31
32 Induced Current-Voltage Hysteresis in $\text{CH}_3\text{NH}_3\text{PbX}_3$ Perovskite Solar Cells. *Nat. Com-*
33
34 *mun.* **2016**, *7*, 10334.
35
36
37 (49) Prochowicz, D.; Frankevičius, M.; Cieślak, A.; Zakeeruddin, S.; Grätzel, M.;
38
39 Lewiński, J. Mechanosynthesis of the Hybrid Perovskite $\text{CH}_3\text{NH}_3\text{PbI}_3$: Characteriza-
40
41 tion and the Corresponding Solar Cell Efficiency. *J. Mater. Chem. A* **2015**, *3*, 20772–
42
43 20777.
44
45
46 (50) Prochowicz, D.; Yadav, P.; Saliba, M.; Sasaki, M.; Zakeeruddin, S.; Lewiński, J.;
47
48 Grätzel, M. Mechanosynthesis of Pure Phase Mixed-Cation $\text{MA}_x\text{FA}_{1-x}\text{PbI}_3$ Hybrid
49
50 Perovskites: Photovoltaic Performance and Electrochemical Properties. *Sustain. En-*
51
52 *ergy Fuels* **2017**, *1*, 689–693.
53
54
55 (51) Rosales, B. A.; Wei, L.; Vela, J. Synthesis and Mixing of Complex Halide Perovskites
56
57 by Solvent-Free Solid-State Methods. *J. Solid State Chem.* **2019**, *271*, 206–215.
58
59
60

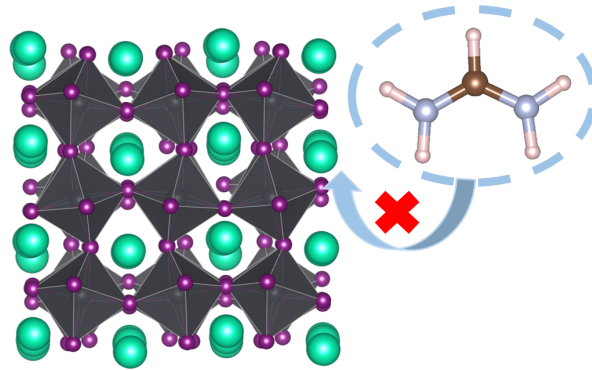
- 1
2
3 (52) Kubicki, D. J.; Prochowicz, D.; Hofstetter, A.; Pechy, P.; Zakeeruddin, S. M.;
4 Grätzel, M.; Emsley, L. Cation Dynamics in Mixed-Cation (MA)_x(FA)_{1-x}PbI₃ Hybrid
5 Perovskites from Solid-State NMR. *J. Am. Chem. Soc.* **2017**, *139*, 10055–10061.
6
7
8
9
10 (53) Kubicki, D. J.; Prochowicz, D.; Hofstetter, A.; Sasaki, M.; Yadav, P.; Bi, D.; Pel-
11 let, N.; Lewiński, J.; Zakeeruddin, S. M.; Grätzel, M., et al. Formation of Stable Mixed
12 Guanidinium-Methylammonium Phases with Exceptionally Long Carrier Lifetimes for
13 High-Efficiency Lead Iodide-Based Perovskite Photovoltaics. *J. Am. Chem. Soc.* **2018**,
14 *140*, 3345–3351.
15
16
17
18
19
20 (54) Kubicki, D. J.; Prochowicz, D.; Hofstetter, A.; Zakeeruddin, S. M.; Grätzel, M.; Em-
21 sley, L. Phase Segregation in Potassium-Doped Lead Halide Perovskites from 39 K
22 solid-state NMR at 21.1 T. *J. Am. Chem. Soc.* **2018**, *140*, 7232–7238.
23
24
25
26
27 (55) Bi, D.; Li, X.; Milić, J. V.; Kubicki, D. J.; Pellet, N.; Luo, J.; LaGrange, T.; Met-
28 traux, P.; Emsley, L.; Zakeeruddin, S. M., et al. Multifunctional Molecular Modulators
29 for Perovskite Solar Cells with over 20% Efficiency and High Operational Stability. *Nat.*
30 *Commun.* **2018**, *9*, 4482.
31
32
33
34
35 (56) Tavakoli, M. M.; Tress, W.; Milić, J. V.; Kubicki, D.; Emsley, L.; Grätzel, M. Addition
36 of Adamantylammonium Iodide to Hole Transport Layers Enables Highly Efficient and
37 Electroluminescent Perovskite Solar Cells. *Energy Environ. Sci.* **2018**, *11*, 3310–3320.
38
39
40
41
42 (57) Kubicki, D. J.; Prochowicz, D.; Pinon, A.; Stevanato, G.; Hofstetter, A.; Zakeerud-
43 din, S. M.; Grätzel, M.; Emsley, L. Doping and Phase Segregation in Mn²⁺- and Co²⁺-
44 Doped Lead Halide Perovskites from ¹³³Cs and ¹H NMR Relaxation Enhancement. *J.*
45 *Mater. Chem. A* **2019**, *7*, 2326–2333.
46
47
48
49
50 (58) Rosales, B. A.; Men, L.; Cady, S. D.; Hanrahan, M. P.; Rossini, A. J.; Vela, J. Persistent
51 Dopants and Phase Segregation in Organolead Mixed-Halide Perovskites. *Chem. Mater.*
52 **2016**, *28*, 6848–6859.
53
54
55
56
57
58
59
60

- 1
2
3 (59) Rosales, B. A.; Hanrahan, M. P.; Boote, B. W.; Rossini, A. J.; Smith, E. A.; Vela, J.
4 Lead Halide Perovskites: Challenges and Opportunities in Advanced Synthesis and
5 Spectroscopy. *ACS Energy Lett.* **2017**, *2*, 906–914.
6
7
8
9
10 (60) Karmakar, A.; Askar, A. M.; Bernard, G. M.; Terskikh, V. V.; Ha, M.; Patel, S.;
11 Shankar, K.; Michaelis, V. K. Mechanochemical Synthesis of Methylammonium Lead
12 Mixed-Halide Perovskites: Unraveling the Solid-Solution Behavior Using Solid-State
13 NMR. *Chem. Mater.* **2018**, *30*, 2309–2321.
14
15
16
17
18 (61) Kubicki, D. J.; Prochowicz, D.; Hofstetter, A.; Zakeeruddin, S. M.; Grätzel, M.; Em-
19 sley, L. Phase Segregation in Cs-, Rb- and K-Doped Mixed-Cation $(\text{MA})_x(\text{FA})_{1-x}\text{PbI}_3$
20 Hybrid Perovskites from Solid-State NMR. *J. Am. Chem. Soc.* **2017**, *139*, 14173–14180.
21
22
23
24
25 (62) Xiang, W.; Wang, Z.; Kubicki, D. J.; Tress, W.; Luo, J.; Prochowicz, D.; Akin, S.;
26 Emsley, L.; Zhou, J.; Dietler, G., et al. Europium-Doped CsPbI₂Br for Stable and
27 Highly Efficient Inorganic Perovskite Solar Cells. *Joule* **2019**, *3*, 205–214.
28
29
30
31
32 (63) Prochowicz, D.; Yadav, P.; Saliba, M.; Kubicki, D. J.; Tavakoli, M. M.; Zakeerud-
33 din, S. M.; Lewiński, J.; Emsley, L.; Grätzel, M. One-step Mechanochemical Incorpor-
34 ation of an Insoluble Cesium Additive for High Performance Planar Heterojunction
35 Solar Cells. *Nano Energy* **2018**, *49*, 523–528.
36
37
38
39
40 (64) Karmakar, A.; Dodd, M. S.; Agnihotri, S.; Ravera, E.; Michaelis, V. K. Cu(II)-Doped
41 Cs₂SbAgCl₆ Double Perovskite: A Lead-Free, Low-Bandgap Material. *Chem. Mater.*
42 **2018**, *30*, 8280–8290.
43
44
45
46
47 (65) Karmakar, A.; Dodd, M. S.; Zhang, X.; Oakley, M. S.; Klobukowski, M.;
48 Michaelis, V. K. Mechanochemical Synthesis of 0D and 3D Cesium Lead Mixed Halide
49 Perovskites. *Chem. Commun.* **2019**, *55*, 5079–5082.
50
51
52
53
54 (66) Even, J.; Pedesseau, L.; Jancu, J.-M.; Katan, C. Importance of Spin–Orbit Coupling in
55
56
57
58
59
60

- Hybrid Organic/Inorganic Perovskites for Photovoltaic Applications. *J. Phys. Chem. Lett.* **2013**, *4*, 2999–3005.
- (67) Umari, P.; Mosconi, E.; De Angelis, F. Relativistic GW calculations on $\text{CH}_3\text{NH}_3\text{PbI}_3$ and $\text{CH}_3\text{NH}_3\text{SnI}_3$ Perovskites for Solar Cell Applications. *Sci. Rep.* **2014**, *4*, 4467.
- (68) Ashari-Astani, N.; Meloni, S.; Salavati, A. H.; Palermo, G.; Grätzel, M.; Rothlisberger, U. Computational Characterization of the Dependence of Halide Perovskite Effective Masses on Chemical Composition and Structure. *J. Phys. Chem. C* **2017**, *121*, 23886–23895.
- (69) Hohenberg, P.; Kohn, W. Inhomogeneous Electron Gas. *Phys. Rev.* **1964**, *136*, B864–B871.
- (70) Kohn, W.; Sham, L. J. Self-Consistent Equations Including Exchange and Correlation Effects. *Phys. Rev.* **1965**, *140*, A1133–A1138.
- (71) Giannozzi, P. et al. QUANTUM ESPRESSO: a Modular and Open-Source Software Project for Quantum Simulations of Materials. *J. Phys. Condens. Matter* **2009**, *21*, 395502.
- (72) Giannozzi, P. et al. Advanced Capabilities for Materials Modelling with Quantum ESPRESSO. *J. Phys. Condens. Matter* **2017**, *29*, 465901.
- (73) Corso, A. D. Pseudopotentials Periodic Table: From H to Pu. *Comput. Mater. Sci.* **2014**, *95*, 337–350.
- (74) Monkhorst, H. J.; Pack, J. D. Special Points for Brillouin-Zone Integrations. *Phys. Rev. B* **1976**, *13*, 5188–5192.
- (75) Alkauskas, A.; Broqvist, P.; Pasquarello, A. Defect Energy Levels in Density Functional Calculations: Alignment and Band Gap Problem. *Phys. Rev. Lett.* **2008**, *101*, 046405.

- 1
2
3 (76) CPMD, <http://www.cpmd.org/>, Copyright IBM Corp 1990-2015, Copyright MPI für
4 Festkörperforschung Stuttgart 1997-2001 (Visited on 02/05/2019).
5
6
7
8 (77) Goedecker, S.; Teter, M.; Hutter, J. Separable Dual-Space Gaussian Pseudopotentials.
9 *Phys. Rev. B* **1996**, *54*, 1703–1710.
10
11
12 (78) Hartwigsen, C.; Goedecker, S.; Hutter, J. Relativistic Separable Dual-Space Gaussian
13 Pseudopotentials from H to Rn. *Phys. Rev. B* **1998**, *58*, 3641–3662.
14
15
16
17 (79) Krack, M. Pseudopotentials for H to Kr Optimized for Gradient-Corrected Exchange-
18 Correlation Functionals. *Theor. Chem. Acc.* **2005**, *114*, 145–152.
19
20
21
22 (80) Nosé, S. A Molecular Dynamics Method for Simulations in the Canonical Ensemble.
23 *Mol. Phys.* **1984**, *52*, 255–268.
24
25
26
27 (81) Nosé, S. A Unified Formulation of the Constant Temperature Molecular Dynamics
28 Methods. *J. Chem. Phys.* **1984**, *81*, 511–519.
29
30
31
32 (82) Hoover, W. G. Canonical Dynamics: Equilibrium Phase-Space Distributions. *Phys.*
33 *Rev. A* **1985**, *31*, 1695–1697.
34
35
36
37
38
39
40
41
42
43
44
45
46
47
48
49
50
51
52
53
54
55
56
57
58
59
60

1
2
3
4
5
6
7
8
9
10
11
12
13
14
15
16
17
18
19
20
21
22
23
24
25
26
27
28
29
30
31
32
33
34
35
36
37
38
39
40
41
42
43
44
45
46
47
48
49
50
51
52
53
54
55
56
57
58
59
60



For Table of Contents Only